Nondestructive evaluation of interface defects in layered media

Gabriele Inglese[*]
IAC M.Picone-CNR
via Madonna del Piano 10
50019 Sesto Fiorentino
Italy
gabriele@fi.iac.cnr.it

Roberto Olmi
IFAC-CNR
via Madonna del Piano 10
50019 Sesto Fiorentino
Italy
r.olmi@ifac.cnr.it

Abstract. In a layered thermal conductor, the inaccessible interface could be damaged by mechanical solicitation, chemical infiltration, aging. In this case, the original thermal properties of the specimen are modified. The defect occurs typically in form of *delamination*. The present paper deals with nondestructive evaluation of interface thermal conductance h from the knowledge of the surface temperature when the specimen is heated in some controlled way. The goal is achieved by expanding h in powers of the thickness of the upper layer. The mathematical analysis of the model produces exact formulas for the first coefficients of h which are tested on simulated and real data. The evaluation of interface flaws comes from reliable approximation of h.

Keywords: imperfect interface, thermal contact conductance, heat equation, inverse problem.

MSC 2020: 35F51 41A99 80A23

1. Introduction

In a layered conductor, the inaccessible interface $\tilde{\Sigma}$ could be damaged by mechanical solicitation, chemical infiltration, aging. In this case, the original thermal properties of the specimen are modified. The present paper deals with nondestructive evaluation of defects in $\tilde{\Sigma}$ from the knowledge of the surface temperature when the specimen is heated by applying a voltage or by means of a lamp system or a laser. Temperature is measured with an infrared camera in the typical framework of Active Thermography [19]. The mathematical model consists of a system of two Boundary Value Problems (BVPs) for the Laplace-transformed heat equation. The evaluation of defects affecting the interface requires the approximate solution of a non linear Inverse Heat Conduction Problem.

---

[*]. Corresponding author

1.1 Layered domains

Consider a composite body made up of two thermally conducting layers $\tilde{B}^+$ and $\tilde{B}^-$ divided by a very thin and irregular interspace $\tilde{S}$ filled up with air or other poorly conductive materials (see Figure 1 (a)). As long as $\tilde{B}^-$ is heated by an external source, heat flows through $\tilde{S}$ mainly in correspondence to possible contact spots between the conducting layers. As strong as the layers are pressed together, their contact area depends on nonflatness and roughness of the contacting surfaces. Assume that the effect of $\tilde{S}$ on heat transfer between the two layers $\tilde{B}^-$ and $\tilde{B}^+$ is equivalent to the effect of a smooth thin interspace S of constant thickness d_S and virtual thermal conductivity κ_S. In this case a model with three layers is obtained ($B^+ \cup S \cup B^-$ see Figure 1 (b)) where the opposite sides of S have different temperature but there is no thermal gap between adjacent layers B^+, S and S, B^-. It is shown in [10] that heat conduction in $B^+ \cup S \cup B^-$ is correctly modeled in terms of transmission conditions on a two-dimensional interface $\tilde{\Sigma}$ that separates the conducting layers. Indeed, the thin domain S shrinks to the surface $\tilde{\Sigma}$ (a rigorous analysis of limits of the form $\lim_{d_S \to 0} \frac{k_S}{d_S}$ in a similar geometry is in [8], Sect 7) so that the specimen is, finally, $\tilde{\Omega} = \tilde{\Omega}^+ \cup \tilde{\Sigma} \cup \tilde{\Omega}^-$ (see, Figure 1 (c)).
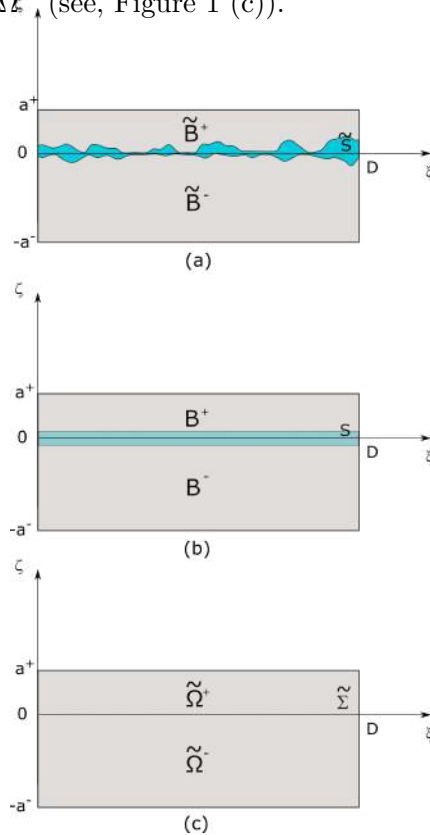

Figure 1: layered domain: from the interspace $\tilde{S}$ to the interface $\tilde{\Sigma}$

1.2 Types of interfaces and thermal parameters

Interfaces can be classified as perfect or imperfect according to their thermal properties [16]. In case of *perfect interfaces*, temperature and normal heat flux are continuous in $\tilde{\Sigma}$ while the model of *Low Conductivity Imperfect* (LCI) interface allows for a temperature jump with continuous heat flux.

The *Thermal Contact Resistance* (TCR) $\bar{r}$ (see for example [12] Ch 3) is a non negative parameter proportional to the temperature gap between the two sides of $\tilde{\Sigma}$. Its inverse $\bar{h} = \frac{1}{\bar{r}}$ is referred to as *Thermal Contact Conductance* (TCC).

In perfect interfaces the parameter $\bar{r}$ is zero (very small in practice) and $\bar{h}$ is infinite (actually large).

In LCIs, the resistance is $\bar{r} >> 0$. In the limit case of infinite $\bar{r}$ the interface is perfectly insulating and $\bar{h} = 0$.

A defect affecting $\tilde{\Sigma}$ gives rise to anomalies in the thermal behavior of the interface. We focus on the case in which the undamaged interface is perfect ($\bar{r}$ is very small) and the defect is an inclusion between the layers (see for example [23]). The occurrence of a similar defect produces locally a larger TCR $r = \bar{r} + \delta r$ ($\delta r > 0$ non constant on $\tilde{\Sigma}$). The extension of TCR and TCC to the perturbed non constant case is not rigorously founded but it is in agreement with experimental data and widely used among practitioners (see for example [1, 26, 2]). Hence, $h = \frac{1}{\bar{r}+\delta r} = \bar{h} + \delta h$ ($\delta h < 0$ non constant on $\tilde{\Sigma}$) plays the role of exchange coefficient in Robin transmission conditions (5) and (6) in section 2. In this case, there is no appreciable temperature gap between the opposite sides of $\tilde{\Sigma}$ except on the damaged area where we expect that the numerical value of $\frac{\kappa_a}{h}$ (κ_a is the thermal conductivity of the inclusion) gives a good approximation of the thickness of the defect [7]. We can reasonably simplify the problem by assuming that the defect is actually a *delamination* described by the graph of a function of two variables whose level sets are convex. More precisely, in applicative literature, "the delamination zone is often taken as a square, circular or elliptical domain so as to confirm a satisfactory compromise between the realistic representation of the geometry of the real delamination and the simple insertion of the artificial damage" [9]. We apply this concept in section 7.2. A detailed analysis of nondestructive inspection of impact-damaged composite structures is in [25]. The interface is usually filled with air. Treating the interface in terms of thermal conductance only is anyhow justified because its size is small enough to prevent the occurrence of convective motions which would require a mixed thermal/fluid model.

1.3 The direct model and the inverse problem

In this section, we describe briefly the specific model and the approach used here to solve the inverse problem. The lower layer $\tilde{\Omega}^-$ is heated by means of thermal flux coming from below, e.g. by a lamp, kept on for a time interval of $\tau_{\max}$ seconds. Heat passes through the interface $\tilde{\Sigma}$ so that the temperature

of $\tilde{\Omega}^+$ changes during heating. Heat transfer through the interface is modeled by means of Robin transmission boundary conditions (see for example [21, 6]). A sequence $\tilde{\psi}$ of temperature maps is taken, in the meanwhile, on the external surface of $\tilde{\Omega}^+$. This setting is usually referred to as *transmission mode* [5] in Long Pulse Thermography. Details of this mathematical model, based on the heat equation in normalized dimensionless variables, are in section 3. In the new variables, layers are named Ω^+ and Ω^- while the interface is Σ and the whole specimen is $\Omega = \Omega^+ \cup \Sigma \cup \Omega^-$.

It is remarkable that h is independent of time (at least in the time scale of $t_{\max}$) so that it is convenient to apply Laplace's transform to equations and boundary conditions (see section 4). In this way we obtain a system of two BVPs for elliptic equations in Ω^+ and Ω^- (connected by Robin transmission conditions) whose solutions U^+ and U^- are the Laplace transform of the temperatures of the two layers. At this point, since our specimen is composed by thin layers, we introduce the formal expansion of h, U^+ and U^- in even powers of the normalized thickness γ of $\tilde{\Omega}^+$. Our goal is to write the coefficients h_k (of the expansion in γ^{2k}) in terms of the available data (incomplete thermal boundary data). We accomplish this task by means of a generalization of Thin Plate Approximation (TPA). In particular, we show that the coefficients of the expansion of the trace of U^- on Σ fulfills a family of Neumann problems for elliptic PDEs at least for $k = 0, 1$ (see (30) and (53)). In this way, transmission conditions for $k = 0, 1$ on the positive side of Σ become ordinary Robin conditions for BVPs in Ω^+ so that we are in a position to derive the explicit expressions of h_0 and h_1 in terms of $\tilde{\psi}$. A similar model has been studied in [3] where a flaw (of unknown depth) is evaluated from the knowledge of a complete set of thermal data at the boundary. A stationary two-dimensional case is studied in [1] using reciprocity functional approach. A problem of *reflection mode* [5] in Long Pulse Thermography of a single layer specimen is solved in [14].

We recall that TPA is a perturbative technique for the computational solution of some inverse problems on thin domains, borrowed from [18]. In [13], TPA is compared with pre-existing methods based on reciprocity functional approach, optimization and regularization [4].

1.4 Simulations and experiments

We apply the method described in section 6 to the nondestructive evaluation of defects affecting the interface of a coated iron slab. We test the first order approximation (i.e. $h \approx h_0 + \gamma^2 h_1$) both in 2D simulations and in case of real data in a full 3D model. The approximation of h (real data are processed) shown in figure 6 improves the reconstruction obtained in [24] where the trace of U^- on Σ is heuristically overwritten by its background temperature.

2. Geometry, notation, direct model and inverse problem

Let $\tilde{\Omega}$ be the parallelepiped $(0, D) \times (0, D) \times (-a^-, a^+)$ in the 3D space (ξ, η, ζ). Let $\tilde{\Omega}^+$ be $(0, D) \times (0, D) \times (0, a^+)$ and $\tilde{\Omega}^-$ be $(0, D) \times (0, D) \times (-a^-, 0)$. Let $\tilde{\Sigma} = \{(\xi, \eta) \in (0, D) \times (0, D) , \zeta = 0\}$. Clearly $\tilde{\Omega} = \tilde{\Omega}^+ \cup \tilde{\Sigma} \cup \tilde{\Omega}^-$.

To fix ideas, assume that $\frac{a^+ + a^-}{D} << 1$. The geometry of the problem is summarized in Figure 2. The thermal behavior of each layer $\tilde{\Omega}^\pm$ is determined by its conductivity $\tilde{\kappa}^\pm$, density $\rho^\pm$ and specific heat $c^\pm$. Heat transfer through the interface $\tilde{\Sigma}$ depends on its thermal contact conductance $\tilde{h}(\xi, \eta)$.

Let $v^\pm(\xi, \eta, \zeta, \tau)$ with $(\xi, \eta, \zeta) \in \tilde{\Omega}^\pm$ and $\tau > 0$ the temperature increase (with respect to an initial and surrounding temperature V_0) in $\tilde{\Omega}^\pm$ obtained by applying, for a time interval $(0, \tau_{\max})$, a heat flux $\tilde{\phi}(\xi, \eta, \tau)$ to $\tilde{\Omega}^-$ (more precisely, $\tilde{\phi}(\xi, \eta, \tau) = 0$ for $\tau > \tau_{\max}$) . Clearly, $v(\xi, \eta, \zeta, 0) = 0$. Assume that the vertical sides of the composite domain are insulated while the horizontal sides exchange heat with the environment. The thermal contact conductances of top $(\zeta = a^+)$ and bottom side $(\zeta = -a^-)$ are the positive constants $\tilde{h}^+$ and $\tilde{h}^-$ respectively.

2.1 The direct model

Given the constant parameters $a^\pm$, D, $\tilde{\kappa}^\pm$, $\rho^\pm$, $c^\pm$ and $\tilde{h}^\pm$ and given interface thermal conductance $\tilde{h}(\xi, \eta)$, the functions $v^\pm$ fulfill an Initial Boundary Value Problem (IBVP) for the heat equation in the composite domain $\tilde{\Omega}$ (we write down this IBVP later in dimensionless variables).

$$(1) \qquad \rho^- c^- v_\tau^- = \tilde{\kappa}^- (v_{\xi\xi}^- + v_{\eta\eta}^- + v_{\zeta\zeta}^-) , \ (\xi, \eta, \zeta) \in \tilde{\Omega}^-, \ \tau > 0,$$

$$(2) \qquad -\tilde{\kappa}^- v_\zeta^-(\xi, \eta, -a^-) + \tilde{h}^- v^-(\xi, \eta, -a^-) = \tilde{\phi}(\xi, \eta, \tau),$$

$$(3) \qquad \rho^+ c^+ v_\tau^+ = \tilde{\kappa}^+ (v_{\xi\xi}^+ + v_{\eta\eta}^+ + v_{\zeta\zeta}^+) , \ (\xi, \eta, \zeta) \in \tilde{\Omega}^+, \ \tau > 0,$$

$$(4) \qquad \tilde{\kappa}^+ v_\zeta^+(\xi, \eta, a^+, \tau) + \tilde{h}^+ v^+(\xi, \eta, a^+, \tau) = 0$$

and $v_\nu^\pm = 0$ on the *vertical* sides of $\tilde{\Omega}^\pm$, with *transmission conditions*

$$(5) \qquad \tilde{\kappa}^- v_\zeta^-(\xi, \eta, 0, \tau) + \tilde{h}(\xi, \eta)(v^-(\xi, \eta, 0, \tau) - v^+(\xi, \eta, 0, \tau)) = 0,$$

$$(6) \qquad \tilde{\kappa}^- v_\zeta^-(\xi, \eta, 0, \tau) = \tilde{\kappa}^+ v_\zeta^+(\xi, \eta, 0, \tau)$$

Initial data are

$$(7) \qquad v^-(\xi, \eta, \zeta, 0) = 0 , \ (\xi, \eta, \zeta) \in \tilde{\Omega}^-,$$

$$(8) \qquad v^+(\xi, \eta, \zeta, 0) = 0 , \ (\xi, \eta, \zeta) \in \tilde{\Omega}^+.$$

2.2 The interface inverse problem

Assumed that $\tilde{h}(\xi, \eta)$ is unknown, the goal is to approximate $\tilde{h}$ by using the knowledge of $\tilde{\phi}$ and the available additional (boundary) dataset $\tilde{\psi}(\xi, \eta, \tau) = v^+(\xi, \eta, a^+, \tau)$ for $\tau \in (0, \tau_{\max})$.

3. Dimensionless variables

We introduce the standard set of dimensionless variables $z = \frac{\zeta}{a^+}$, $x = \frac{\xi}{D}$, $y = \frac{\eta}{D}$ and $t = \frac{\tau}{T}$ where $T = \frac{\rho^+ c^+ D^2}{\tilde{\kappa}^+}$. We set also $\kappa^\pm = \frac{\tilde{\kappa}^\pm}{D^2}$ and $\beta = \frac{\alpha^-}{\alpha^+}$ where the numbers $\alpha_\pm = \frac{\kappa_\pm}{\rho_\pm c_\pm}$ are the diffusivities of upper and lower slabs respectively.

Rewrite the geometry of the problem in the new variables. Here $b = \frac{a^-}{a^+}$.
Let Ω be the parallelepiped $(0,1) \times (0,1) \times (-b,1)$ in the 3D space (x,y,z).
Let Ω^+ be $(0,1) \times (0,1) \times (0,1)$ and Ω^- be $(0,1) \times (0,1) \times (-b,0)$.
Let $\Sigma = \{(x,y) \in (0,1) \times (0,1) \ , \ z = 0\}$. Clearly $\Omega = \Omega^+ \cup \Sigma \cup \Omega^-$.
Define

$$
\begin{aligned}
u^\pm(x,y,z,t) &\equiv v^\pm(Dx, Dy, a^+z, Tt), \\
\psi(x,y,t) &= \tilde{\psi}(Dx, Dy, Tt), \\
\gamma\phi(x,y,t) &= \tilde{\phi}(Dx, Dy, Tt), \\
\gamma h(x,y) &= \tilde{h}(Dx, Dy).
\end{aligned}
$$

(9)

As for the (known a priori) constant thermal conductances of top and bottom sides of Ω, we set $\tilde{h}^+ = \gamma h^+$ and $\tilde{h}^- = \gamma h^-$ respectively. The scaling factor γ (defined at the end of section 2.1) is functional to the power expansions of $u^\pm$ and h in what follows.

In dimensionless variables and taking into account (9), system (1)-(8) becomes

$IBVP^-$

(10) $\qquad \gamma^2 u_t^- = \beta\gamma^2(u_{xx}^- + u_{yy}^-) + \beta u_{zz}^- \ , \ (x,y,z) \in \Omega^-, \ t > 0,$

(11) $\qquad -D\kappa^- u_z^-(x,y,-b,t) + \gamma^2 h^- u^-(x,y,-b,t) = \gamma^2\phi(x,y,t)$

($u_\nu = 0$ on the *vertical* sides of Ω^-)

$IBVP^+$

(12) $\qquad \gamma^2 u_t^+ = \gamma^2(u_{xx}^+ + u_{yy}^+) + u_{zz}^+ \ , \ (x,y,z) \in \Omega^+, \ t > 0,$

(13) $\qquad D\kappa^+ u_z^+(x,y,1) + \gamma^2 h^+ u^+(x,y,1) = 0$

($u_\nu = 0$ on the *vertical* sides of Ω^+)

with *transmission conditions*

(14) $\qquad D\kappa^- u_z^-(x,y,0) + \gamma^2 h(x,y)(u^-(x,y,0) - u^+(x,y,0)) = 0$

(15) $\qquad \kappa^- u_z^-(x,y,0) = \kappa^+ u_z^+(x,y,0).$

Initial data are

(16) $$u^-(x, y, z, 0) = 0 \ , \ (x, y, z) \in \Omega^-,$$

(17) $$u^+(x, y, z, 0) = 0 \ , \ (x, y, z) \in \Omega^+.$$

Remark. If ϕ and h are continuous functions and $H^1(\Omega)$ is a product Hilbert space equipped with a suitable norm, the system (10)-(16) admits a unique solution $(u^+, u^-) \in L^2(0, T; H^1(\Omega))$, stable with respect to error on h (see [15]).

4. Laplace transform of the direct problem

First, define (for all real positive numbers s) the Laplace transform of $u^\pm(x, y, z, t)$ as

(18) $$U^{s\pm}(x, y, z) = \int_0^\infty u^\pm(x, y, z, t) e^{-st} dt$$

while

$$\Phi^s(x, y) = \int_0^\infty \phi(x, y, t) e^{-st} dt.$$

We know that the bounded function $u(x, y, 0, t)$ is decreasing for $t > t_{\max} + \delta t$ where $\delta t > 0$ depends on thickness and diffusivity of the specimen. The temperature data $\psi(x, y, t)$ can be extended formally for $t > t_{\max}$ to a bounded function ψ_∞ decreasing to zero without any sensitive effect in the calculation of the Laplace transform of ψ_∞ (in a suitable range of s). Hence, in what follows it is

$$\Psi^s(x, y) = \int_0^\infty \psi_\infty(x, y, t) e^{-st} dt.$$

Standard calculations change (10)-(16) into the following system of elliptic BVPs

BVP^-

(19) $$\gamma^2 s U^{s-} = \beta\gamma^2(U^s_{xx} + U^-_{yy}) + \beta U^s_{zz} \ , \ (x, y, z) \in \Omega^-,$$

(20) $$- D\kappa^- U^s_z(x, y, -b) + \gamma^2 h^- U^{s-}(x, y, -b) = \gamma^2 \Phi^s(x, y)$$

and $U^s_\nu = 0$ on the *vertical* sides of Ω^-

BVP^+

(21) $$\gamma^2 s U^{s+} = \gamma^2(U^{s+}_{xx} + U^{s+}_{yy}) + U^{s+}_{zz} \ , \ (x, y, z) \in \Omega^+,$$

(22) $$D\kappa^+ U^{s+}_z(x, y, 1) + \gamma^2 h^+ U^{s+}(x, y, 1) = 0$$

and $U^{s+}_\nu = 0$ on the *vertical* sides of Ω^+ with *transmission conditions*

(23) $$D\kappa^- U^s_z(x, y, 0) + \gamma^2 h(x, y)(U^{s-}(x, y, 0) - U^{s+}(x, y, 0)) = 0,$$

(24) $$\kappa^- U^s_z(x, y, 0) = \kappa^+ U^{s+}_z(x, y, 0).$$

In what follows $U^{s\pm}$, Ψ^s and Φ^s are written simply $U^\pm$, Ψ and Φ. The dependence on the parameter s is implicit. The actual choice of values of s is discussed in section 7.1.

5. The inverse problem

After introducing dimensionless variables and applying Laplace's transform, the inverse problem defined in the end of section 2 is formulated the following way:

Interface Inverse Problem Assumed that the coefficient $h(x, y)$ in (23) is unknown, it must be recovered from the knowledge of Φ and the available additional (boundary) data $\Psi(x, y) = U^+(x, y, 1))$.

Mathematical remark It is immediate to realize that the external flux $U_\nu^\pm$ is known on the whole boundary of Ω while $U^\pm$ is given only on the top boundary of Ω^+ (incomplete Neumann to Dirichlet (NTD) map). A wide mathematical literature about uniqueness and stability of solutions of inverse problems for parabolic and elliptic PDEs is available, but we did not find any theorem fitting our Interface Inverse Problem in presence of incomplete NTD map. A rigorous solution of this aspect of the problem is out of the goal of the present research. Actually, this is a work in progress starting from the useful suggestions in [22] (a single domain instead of a layered one) and [11] (full NTD map, continuous temperature and discontinuous flux at the interface).

6. Thin plate approximation

First, we stress that, when h is given, the solutions U^+ and U^- of (19)-(23) depend on γ^2. If also h is unknown, any approximation based on the direct model (19)-(23) also depends on γ^2. Since the parameter γ is assumed small, we introduce the following formal expansions:

$$
\begin{aligned}
U^-(x, y, z) &= U_0^-(x, y, z) + \gamma^2 U_1^-(x, y, z) + ..., \\
U^+(x, y, z) &= U_0^+(x, y, z) + \gamma^2 u_1^+(x, y, z) + ..., \\
h(x, y) &= h_0(x, y) + \gamma^2 h_1(x, y) + ...
\end{aligned}
$$
(25)

6.1 Order zero of the expansion of h

Consider the terms of order zero:

$$U_{0zz}^- = 0,$$

for all (x,y,z), and

$$U_{0z}^-(x, y, -b) = U_{0z}^-(x, y, 0) = U_{0z}^+(x, y, 0) = U_{0z}^+(x, y, 1) = 0.$$

It means that U_0^- and U_0^+ do not depend on z.

First order terms are:

$$U_{1z}^-(x,y,0) = -\frac{h_0(x,y)}{D\kappa^-}(U_0^-(x,y) - U_0^+(x,y)),$$

$$U_{1z}^+(x,y,0) = \frac{\kappa^-}{\kappa^+}U_{1z}^-(x,y,0),$$

(26)
$$U_{1z}^-(x,y,-b) = \frac{h^-}{D\kappa^-}U_0^-(x,y) - \frac{\Phi}{D\kappa^-},$$

$$U_{1z}^+(x,y,1) = -\frac{h^+}{D\kappa^+}U_0^+(x,y),$$

$$U_{1zz}^- = \frac{s}{\beta}U_0^- - (U_{0xx}^- + U_{0yy}^-),$$

$$U_{1zz}^+ = sU_0^+ - (U_{0xx}^+ + U_{0yy}^+).$$

Since $f_z(a_2) = f_z(a_1) + \int_{a_1}^{a_2} f_{zz}(s)ds$, we have

(27) $$-h_0(U_0^- - U_0^+) + h^+U_0^+ + D\kappa^+ sU_0^+ - D\kappa^+\Delta U_0^+ = 0$$

and

(28) $$h_0(U_0^- - U_0^+) + h^-U_0^- - \Phi + D\kappa^-\frac{bs}{\beta}U_0^- - bD\kappa^-\Delta U_0^- = 0.$$

The sum of the last two equation does not depend on the unknown $h_0(x,y)$. Hence, if we assume

(29) $$U_0^+(x,y) = \Psi(x,y)$$

(i.e. $U_k^+(x,y,1) = 0$ for $k > 0$) we have the following elliptic PDE in $U_0^-(x,y,t)$

(30) $$(\frac{h^-}{D\kappa^-} + \frac{bs}{\beta})U_0^- - b\Delta U_0^- = F_0$$

where

(31) $$F_0(x,y) = \frac{\Phi(x,y)}{D\kappa^-} - (\frac{h^+}{D\kappa^-} + \frac{\kappa^+}{\kappa^-}s)\Psi(x,y) + \frac{\kappa^+}{\kappa^-}\Delta\Psi$$

with Neumann boundary conditions

(32) $$U_{0x}^-(0,y) = U_{0x}^-(1,y) = U_{0y}^-(x,0) = U_{0y}^-(x,1) = 0.$$

Hence, solving (27), we obtain

(33) $$h_0(x,y) = \frac{(h^+ + D\kappa^+ s)\Psi(x,y) - D\kappa^+\Delta\Psi(x,y)}{U_0^- - \Psi}.$$

6.2 First order of the expansion of h

In what follows, $Lf = f_{xx} + f_{yy}$. We derive the following first order relation in Ω^+:

$$(34) \qquad U_{1zz}^+ = A_0^+(x, y),$$

where

$$(35) \qquad A_0^+(x, y) = s\Psi(x, y) - L\Psi(x, y)$$

so, that

$$(36) \qquad \begin{aligned} U_{1z}^+(x, z) &= A_0^+(x, y)z + B_0^+(x, y), \\ U_1^+(x, z) &= A_0^+(x, y)\frac{z^2}{2} + B_0^+(x, y)z + C_0^+(x, y), \end{aligned}$$

where

$$(37) \qquad B_0^+(x, y) = -\frac{h_0(x, y)}{D\kappa^+}(U_0^-(x, y) - \Psi(x, y)).$$

Since we assumed $U_0^+(x, y) = U^+(x, y, 1) = \Psi(x, y)$ (see (29), it is $U_1^+(x, y, 1) \equiv 0$ so that

$$(38) \qquad C_0^+(x, y) = -A_0^+(x, y)\frac{1}{2} - B_0^+(x, y)$$

and

$$(39) \qquad U_1^+(x, y, z) = A_0^+(x, y)\frac{z^2 - 1}{2} + B_0^+(x, y)(z - 1).$$

Analogously, in Ω^- we have

$$(40) \qquad U_{1zz}^- = A_0^-(x, y)$$

with

$$(41) \qquad A_0^-(x, y) = \frac{s}{\beta}U_0^-(x, y) - LU_0^-(x, y).$$

so, that

$$(42) \qquad \begin{aligned} U_{1z}^- &= A_0^-(x, y)z + B_0^-(x, y), \\ U_1^-(x, y, z) &= A_0^-(x, y)\frac{z^2}{2} + B_0^-(x, y)z + C_0^-(x, y), \end{aligned}$$

where

$$(43) \qquad B_0^-(x, y) = -\frac{h_0(x, y)}{D\kappa^-}(U_0^-(x, y) - \Psi(x, y)).$$

Observe that the term $U_1^-(x, y, 0) = C_0^-(x, y)$ is still undetermined and it will be obtained by solving an equation having the same form of (30).

6.3 An equation for C_0^-

Second order terms in equations (19) and (21) are

$$U_{2zz}^+ = A_1^+(x, y, z) \tag{44}$$

and

$$U_{2zz}^- = A_1^-(x, y, z), \tag{45}$$

where

$$A_1^+(x, y, z) = sU_1^+(x, y, z) - LU_1^+(x, y, z) \tag{46}$$

and

$$A_1^-(x, y, z) = \frac{s}{\beta}U_1^-(x, y, z) - LU_1^-(x, y, z). \tag{47}$$

As for boundary conditions, we have

$$
\begin{aligned}
U_{2,z}^+(x, y, 1) &= -\frac{h^+}{D\kappa^+}U_1^+(x, y, 1) \equiv 0 \quad from \ (29), \\
U_{2,z}^-(x, y, -b) &= \frac{h^-}{D\kappa^-}U_1^-(x, y, -b), \\
U_{2,z}^-(x, y, 0) &= -\frac{h_1(x, y)}{D\kappa^-}(U_0^-(x, y) - \Psi(x, y)) \\
&\quad - \frac{h_0(x, y)}{D\kappa^-}(U_1^-(x, y, 0) - U_1^+(x, y, 0)), \\
U_{2,z}^+(x, y, 0) &= -\frac{h_1(x, y)}{D\kappa^+}(U_0^-(x, y) - \Psi(x, y)) \\
&\quad - \frac{h_0(x, y)}{D\kappa^+}(U_1^-(x, y, 0) - U_1^+(x, y, 0)).
\end{aligned}
\tag{48}
$$

In order to lighten the notation, in what follows we stress the dependance on the variable z only. Since

$$U_{2z}^+(1) = U_{2z}^+(0) + \int_0^1 U_{2zz}^+(z)dz$$

and

$$U_{2z}^-(0) = U_{2z}^-(-b) + \int_{-b}^0 U_{2zz}^-(z)dz,$$

we have (recall that we assumed $U_1^+(x, y, 1) = 0$)

$$-h_1(U_0^- - \Psi) - h_0(C_0^- + A_0^+\frac{1}{2} + B_0^+) + D\kappa^+ \int_0^1 (sU_1^+(z) - LU_1^+(z))dz = 0 \tag{49}$$

and

$$- h_1(U_0^- - \Psi) - h_0(C_0^- + \frac{A_0^+}{2} + B_0^+)$$

$$(50) \qquad = h^- U_1^-(-b) + D\kappa^- \int_{-b}^0 (\frac{s}{\beta} U_1^-(z) - LU_1^-(z))dz.$$

A substitution gives

$$h^- U_1^-(-b) + D\kappa^- \int_{-b}^0 (\frac{s}{\beta} U_1^-(z) - LU_1^-(z))dz$$

$$(51) \qquad + D\kappa^+ \int_0^1 (sU_1^+(z) - LU_1^+(z))dz = 0.$$

We plug in (51) the expressions (derived in previous section)

$$(52) \qquad U_1^+(x, y, z) = A_0^+(x, y)\frac{z^2 - 1}{2} + B_0^+(x, y)(z - 1),$$

$$U_1^-(x, y, z) = A_0^-(x, y)\frac{z^2}{2} + B_0^-(x, y)z + C_0^-(x, y),$$

where $A_0^{\pm}$ and $B_0^{\pm}$ are known . We get the following equation in C_0^-:

$$(53) \qquad (\frac{h^-}{D\kappa^-} + \frac{bs}{\beta})C_0^- - bLC_0^- = F_1$$

where

$$(54) \qquad F_1(x, y) = \frac{\kappa^+}{\kappa^-} N_3 + N_2 + \frac{h^-}{D\kappa^-} N_1$$

where

$$N_1 = -A_0^+(x, y)\frac{b^2}{2} + B_0^+(x, y)b,$$

$$N_2 = -\frac{s}{\beta}(\frac{-b^3}{6} A_0^-(x, y) - \frac{b^2}{2} B_0^-(x, y)) + (\frac{b^3}{6} LA_0^-(x, y) - \frac{b^2}{2} LB_0^-(x, y)),$$

$$N_3 = +\frac{s}{3} A_0^+ + \frac{s}{2} B_0^+ - \frac{LA_0^+}{3} - \frac{LB_0^+}{2}$$

with Neumann boundary conditions

$$(55) \qquad C_{0x}^-(0, y) = C_{0x}^-(1, y) = C_{0y}^-(x, 0) = C_{0y}^-(x, 1) = 0.$$

Finally, we get

$$(56) \qquad h_1 = \frac{-h_0(C_0^- + \frac{A_0^+}{2} + B_0^+) - D\kappa^+ s(\frac{A_0^+}{3} + \frac{B_0^+}{2}) - D\kappa^+(\frac{LA_0^+}{3} + \frac{LB_0^+}{2})}{U_0^- - \Psi}$$

and, consequently, we have the first order thin plate approximation of h

$$(57) \qquad h(x, y) \approx h_0(x, y) + \gamma^2 h_1(x, y).$$

7. Simulations and inversion of real data

Figure 2 shows the geometry of the two-dimensional model used for testing the TPA solution (57), i.e. equations (33) and (56).
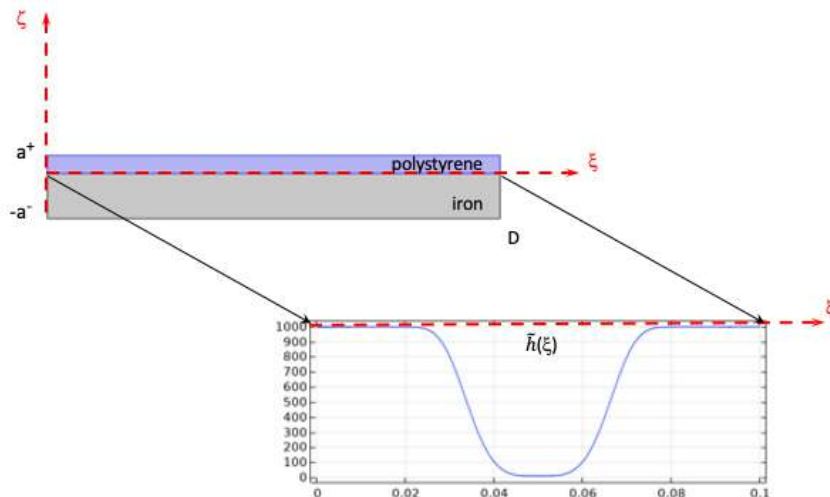

Figure 2: 2D model

A slab of (non-expanded) polystyrene, having thermal conductivity $\tilde{\kappa}^+ = 0.12 \, \mathrm{Wm^{-1}K^{-1}}$, density $\rho^+ = 1050 \, \mathrm{kg \, m^3}$ and specific heat $c^+ = 1100 \, \mathrm{J \, kg^{-1}K^{-1}}$, is superimposed to an iron slab ($\tilde{\kappa}^- = 80 \, \mathrm{Wm^{-1}K^{-1}}$, $\rho^- = 7800 \, \mathrm{kg \, m^3}$, $c^- = 500 \, \mathrm{J \, kg^{-1}K^{-1}}$). The imperfect contact in the central region is simulated by a thermal resistance among the slabs, i.e. by an heat exchange coefficient $h(x)$ whose value is high ($1000 \, \mathrm{W \, m^2 \, K^{-1}}$) where the resistance is negligible and low ($10 \, \mathrm{W \, m^2 \, K^{-1}}$) where the contact is bad. This kind of representation has been demonstrated to approximate reasonably well, for example, a detachment creating an air gap between the two slabs. The assumed shape of $\tilde{h}(\xi)$ is:

$$\tilde{h}(\xi) = H_a - H_b e^{-\theta(\xi - D/2)^4}$$

with $H_a = 1000$, $H_b = 990$, $\theta = 10^7$, this last to obtain an extension of the detachment region of the order of 2 cm.

The 2D model is used to simulate the production of "experimental" data on the upper surface $\zeta = a^+$, when the bottom surface $\zeta = -a^-$ is uniformly heated by a constant flux $\tilde{\phi}$. On that surface is also $h^- = 0$, because $\tilde{\phi}$ is the net flux across it. The direct problem is solved by the finite element method (FEM).

7.1 Reconstruction procedure

After the transformation into dimensionless variables, we fix a real value of the frequency parameter s and compute the Laplace transform of the data. The choice of s does not appear to be critical at all. In fact, a reasonable approach is to choose s high enough to make the product $\psi(x,t)\exp(-st)$ close to zero for any value of the coordinate x, but not too high to lose the information in the data. If, in the transformed t variable, s is such that the exponential becomes, say, 5×10^{-6} for $t = t_{\max}$, this means that: $s = \frac{6\log 10 - \log 5}{t_{\max}}$ or, in terms of the actual time τ, $s = \frac{D^2(6\log 10 - \log 5)}{a^+\tau_{\max}}$. If $\tau_{\max} = 300\ s$, as in the simulation, $s \approx 4000$. With such an s value, for instance, the product $\Psi(x,t)\exp(-st)$ far from the damage (i.e. in values of x corresponding to higher temperatures) is like in Figure 3.
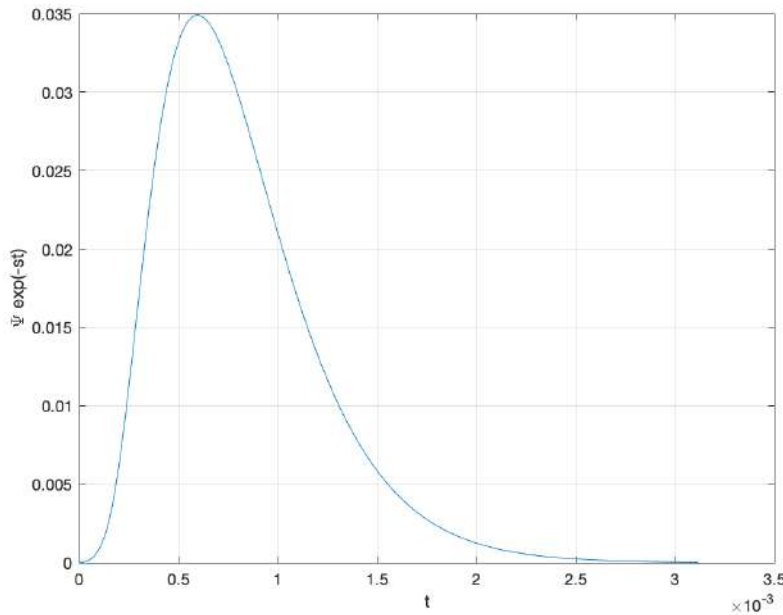

Figure 3: Test of Laplace transform

The numerical procedure involves the following steps.

1. Laplace transformation of the time-dependent data. $\tilde{\psi}(\xi,\tau)$, defined on the line $\xi \in [0, D]$ for $\tau > 0$ is transformed into $\psi(x,t)$ in the dimensionless variables introduced in section 3. Furthermore, $\Psi(x)$ is the Laplace transformation of ψ at the chosen s value. In this phase, the derivative Ψ_{xx} is also computed, by performing a smoothing on the first-order derivative Ψ_x.

2. Ψ and Ψ_{xx} are used to compute the function $F(x)$, allowing the computational solution of the differential equation for U_0^-: $\frac{bs}{\beta}U_0^- - bU_{0xx}^- = F(x)$, where h^- has been taken 0 as in the direct problem. The result, U_0^-, is stored and used to compute the zero-order heat exchange by (33).

3. The third steps computes the coefficients $A_0^{\pm}$, $B_0^{\pm}$, C_0^+, $A_{0xx}^{\pm}$ and $B_{0xx}^{\pm}$, necessary to obtain the function $F_1(x)$ needed to solve the unidimensional equation in C_0^-.

4. The last step numerically solves $\frac{bs}{\beta}C_0^- - bC_{0xx}^- = F_1(x)$ and allows to compute the first-order heat exchange coefficient.

At the end of the procedure, we are able to compute $h(x)$ by means of (57) and, eventually, $\tilde{h}(x) = \gamma h(x)$. The result is shown in Figure 4.
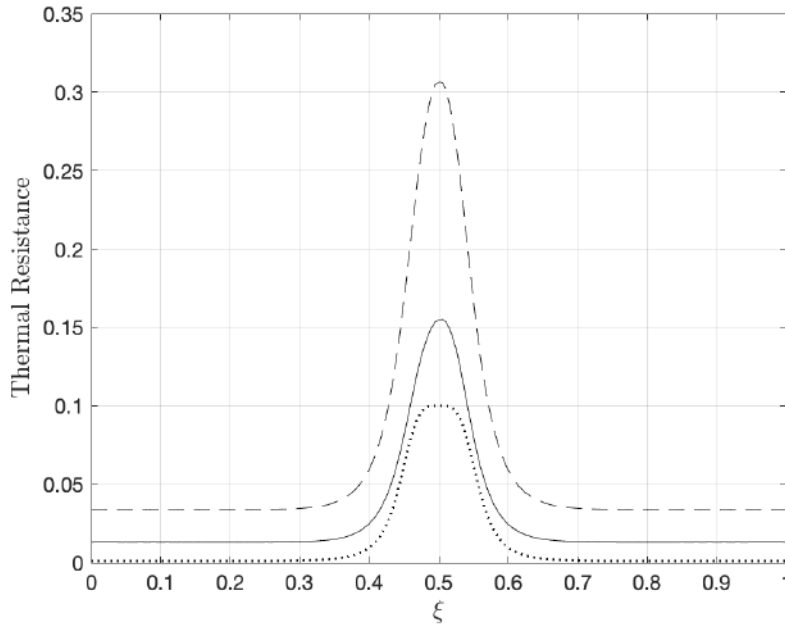

Figure 4: Reconstructed thermal resistance: zero-order $\tilde{h}_0^{-1}$ (dashed line) and first-order $(\tilde{h}_0 + \gamma^2\tilde{h}_1)^{-1}$ (solid line)

Figure 4 superimposes the true, unknown thermal resistance at the interface $\zeta = 0$ (dotted line) with those computed at zero and first order (dashed and solid line, respectively).

7.2 Experimental data

The inversion procedure outlined in the previous sections has been applied to real experimental data taken from [24] where zero order TPA had been computed starting from a rough heuristic evaluation of the temperature of the lower face of the interface. A composite solid consisting in the superposition of two parallelepipeds of square section are heated from below while a thermographic camera acquires thermal shots from above, at a rate of two photograms per second. The lower plate is made of iron ($\kappa_- = 80\ \frac{W}{m\ ^\circ K}$, $c_- = 500\ \frac{J}{Kg\ ^\circ K}$, $\rho_- = 7800\ \frac{Kg}{m^3}$) while the upper one is realized in non expanded polystyrene ($\kappa_+ = 0.12\ \frac{W}{m\ ^\circ K}$, $c_+ = 1100\ \frac{J}{Kg\ ^\circ K}$, $\rho_+ = 1050\ \frac{Kg}{m^3}$). The side of the squares is $D = 10\ cm$. The thicknesses of the lower and upper plates are $a_+ = 0.4\ cm$ and $a_- = 1.0\ cm$, respectively.

A square dig of side 2.0 cm and thickness $\delta = 0.2\ cm$ was made in the center of the iron plate to simulate the imperfect contact at the metal/plastic interface. Heating was provided by fixing a thermal wire electrical resistance on the iron bottom surface by means of aluminium tape. The resistance is connected to a DC power supply that provided 18 W (3.6 V × 5.0 A). Such a condition can be simply simulated by a constant flux $\tilde{\phi}$ at $z = -a^-$, i.e. mathematically by a Neumann condition there. Such a simplification does not affect the temperature behavior with the exception of very early times.

The procedure for computing $\tilde{\phi}$ is the following.

1. Record the temperature values versus time on a number of positions "far" from the damaged region (easily visible, although qualitatively, from thermal images at a suitable time). Those temperatures should, in principle, be very close to one another. Compute the average value as a function of time.

2. Obtain $\tilde{\phi}$ in the unidimensional problem to obtain a good agreement among $\tilde{u}(a^+, t)$ and the experimental values of the previous item.

The other parameters involved in the TPA formula are known, or readily available, being the measured temperature, the thermo-physical characteristics of the materials involved and the geometric quantities. The heat exchange h^+ at the surface $z = a^+$ can be guessed or obtained experimentally [20] but, anyway, it is not a critical one.

Figure 5 compares, on a section $\eta = 0$, the actual thickness of the rectangular defect (dotted line) with those obtained by the TPA procedure at order zero (dashed line) and one (solid line). The curves actually represent a smooth fitting of the quantity obtained by the inversion. It clearly appears that two terms of the expansion are sufficient to have a good quantitative estimate of the damage depth. The width of the square dig is also reasonably obtained, with soft sides (instead of sharp ones) as commonly happens in problems involving heat diffusion.

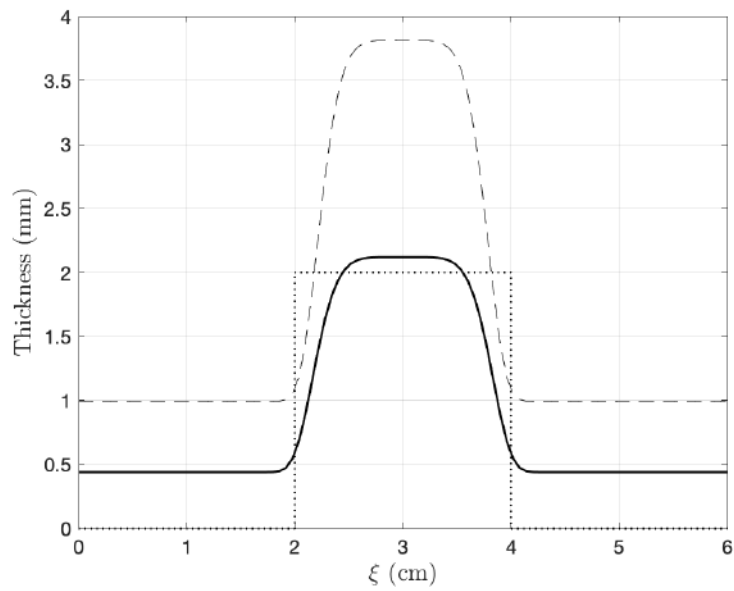Figure 6 shows a 3D reconstruction of the defect.

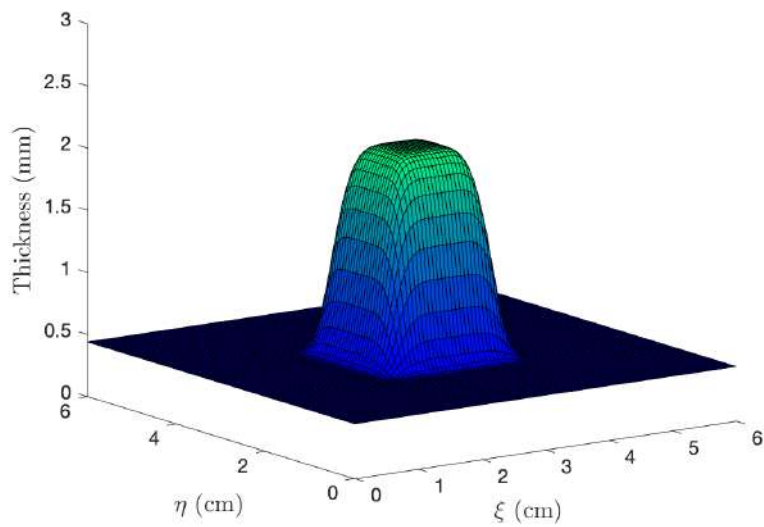Figure 5: Reconstructed thickness: actual value (dotted line), zero-order (dashed line) and first-order (solid line)

Figure 6: 3D reconstruction of the defect thickness

Remark. The dimensionless parameter $\gamma = \frac{a^+}{D}$ gives a measure of how much $\tilde{\Omega}^+$ is "geometrically thin". The slabs $\tilde{\Omega}^+$ and $\tilde{\Omega}^-$ can be considered "thermally thin" when their Biot numbers $Bi^\pm = \frac{a^\pm(\tilde{h}^\pm)}{\tilde{\kappa}^\pm}$ are much smaller than one. A value $Bi \approx 0.1$ is often assumed as a limit value for thermal thinness [12], in the context of the applicability of the well known lumped capacitance method used to approximated the temperature behavior in a solid where the spatial uniformity of the temperature is not violated at any time instant. Here, the meaning of the Biot number is somewhat different: it can be easily demonstrated by a Taylor expansion of the temperature on the domain $\tilde{\Omega}^+$ that if $Bi << 1$ the zero-order term of the TPA is sufficient to obtain an approximation for the exchange coefficient h at the interface. In the case at hand is $Bi^+ \approx 0.17$, so at least one more term of the TPA is needed.

7.3 A remark on Laplace transformation

The recourse to Laplace transformation of the data and, consequently, of the equations involved in the inversion has several practical advantages. As the investigated quantity (damage thickness, thermal resistance, or equivalent heat exchange at the interface) is inherently not time dependent, a time-domain approach should require to identify a characteristic time, or a time range, where such quantity appears to be nearly time-independent. This means that we are forced to solve the problem for all experimental times with a view to discard the most of them. In other words, we do not exploit all the information available in the data.

Laplace transformation, on the other hand, uses the whole available data, by performing a sort of weighted average with exponential weights. Indeed, once the Laplace parameter s has been chosen as discussed in section 7.1, data can be truncated at a previous time, say 200 seconds instead of 300, with a negligible effect on the final result. That is perfectly consistent with the weighted-average interpretation just introduced.

8. Conclusions

This paper deals with nondestructive evaluation of detachment-like defects affecting highly conductive inaccessible interface in the layered specimen Ω. Such defects give rise locally to a thermal resistance r whose imaging gives the required evaluation of the flaw.

The method proposed is based on the expansion

$$h = \frac{1}{r} = h_0 + \gamma^2 h_1 + O(\gamma^4),$$

where γ is the normalized thickness of the upper layer of the specimen Ω. The coefficients h_0 and h_1 are explicitly calculated by means of a perturbative method extending to layered objects a technique, known as Thin Plate Approximation, widely used to solve inverse problems in slabs.

The mathematical novelty consists in the setting of the elliptic BVPs (30) and (53) on the interface whose solutions are the coefficients of the expansion

$$(58) \qquad U^-(x,y,0) = U_0^-(x,y) + \gamma^2 U_1^-(x,y) + O(\gamma^4).$$

Once we know $U^-(x,y,0)$, the problem should be reduced to the determination of the Robin coefficient in the inaccessible side of a slab. As for computation, a quite challenging step is the numerical evaluation of the derivatives of data function Ψ required to get h_0 and h_1.

Future work is mainly in the following two directions:

(i) to obtain a better theoretical foundation of the inverse problem (stability estimates, existence and uniqueness);

(ii) to fit the method to different real objects (curved geometries, failures of insulating interfaces)

References

[1] L.A.S. Abreu, M.J. Colaco, H.R.B. Orlande, C.J.S. Alves, *Thermography detection of contact failures in double layered materials using the reciprocity functional approach*, Applied Thermal Engineering, 100 (2016), 1173-1178.

[2] F. Bozzoli, L. Cattani, A. Mocerino, S. Rainieri, I. Tougri, M.J. Colaco, *Characterisation of the heat transfer in displaced enhancement devices by means of inverse problem approach applied to IR images,* Quantitative InfraRed Thermography Journal, 18 (2021), 108-126.

[3] A. Bendada, F. Erchiqui, M. Lamontagne, *Pulsed thermography in the evaluation of an aircraft composite using 3D thermal quadrupoles and mathematical perturbations,* Inverse Problems, 21 (2005), 857-877.

[4] M.J. Colaco, C.J.S. Alves, F. Bozzoli, *The reciprocity function approach applied to the non-intrusive estimation of spatially varying internal heat transfer coefficients in ducts: numerical and experimental results,* International Journal of Heat and Mass Transfer, 90 (2015), 1221-1231.

[5] C. Meola, G.M. Carlomagno, L. Giorleo, *Geometrical limitation to detection of defects in composites by means of infrared thermography,* J Nondestruct Eval, 23 (2004,) 125-132.

[6] A. Cangiani, E.H. Georgoulis, Y.A. Sabawi, *Adaptive discontinuous Galerkin methods for elliptic interface problems,* Math. Comp. 87 (2018), 2675-2707.

[7] H.S. Carslaw, J.C. Jaeger, *Conduction of heat in solids,* Clarendon Press, Oxford, 1959.

[8] C. Dapogny, M.S. Vogelius, *Uniform asymptotic expansion of the voltage potential in the presence of thin inhomogeneities with arbitrary conductivity,* Chin. Ann. Math., 38B (2017), 293-344.

[9] I. Feddalp, A. Khamlichi, *Delamination buckling of a laminated composite shell panel using cohesive zone modelling,* International Review of Applied Sciences and Engineering, 13 (2022), 228-238.

[10] Z. Hashin, *Thin interphase/imperfect interface in conduction,* Journal of Applied Physics, 89 (2001), 2261.

[11] B. Harrach, H. Meftahi, *Global uniqueness and Lipschitz-stability for the inverse Robin transmission problem,* SIAM Journal on Applied Mathematics, 79.2 (2019), 525-550.

[12] F.P. Incropera, D.P. Dewitt, T.L. Bergman, A.S. Lavine, *Principles of heat and mass transfer,* ISV 7th Edition Wiley, Singapore 2003.

[13] G. Inglese, R. Olmi, *Nondestructive evaluation of spatially varying internal heat transfer coefficients in a tube,* International Journal of Heat and Mass Transfer, 108 (2017), 90-96.

[14] G. Inglese, R. Olmi, S. Priori, *A procedure for detecting hidden surface defects in a thin plate by means of active thermography,* J Nondestruct Eval, 61 (2017).

[15] G. Inglese, R. Olmi, *A note about the well-posedness of an Initial Boundary Value Problem for the heat equation in a layered domain,* to appear in Rendiconti Istituto Matematico Universita di Trieste, 2022.

[16] A. Javili, Kaessmair, S.P. Steinmann, *General imperfect interfaces,* Comput. Methods Appl. Mech. Engrg., 275 (2014), 76-97.

[17] J.C. Krapez, *La camera photothermique-partie I: Principe, modelisation, application a la detection de fissures,* Instrumentation Mesure Metrologie, 1 (2001), 9-39.

[18] P. Kaup, F. Santosa, M. Vogelius, *Method for imaging corrosion damage in thin plates from electrostatic data,* Inverse Problems, 12 (1996), 279.

[19] X.P.V. Maldague, *Theory and practice of infrared technology for nondestructive testing,* John Wiley and Sons, New York, 2001.

[20] R. Olmi, G. Inglese, *Measurement of the external parameters in quantitative active thermography,* Meas. Sci. Technol., 28 (2017), 105403.

[21] R. Perrussel, C. Poignard, *Asymptotic expansion of steady-state potential in a high contrast medium with a thin resistive layer,* Appl. Math. Comp., 221 (2013), 48-65.

[22] A. Prilepko, A.B. Kostin, *Boundary control of heat conduction,* Comput. Math. Model., 7 (1996), 427-430.

[23] A. Ratsakou, A. Skarlatos, C. Reboud, D. Lesselier, *Shape reconstruction of delamination defects using thermographic infrared signals based on an enhanced Canny approach,* Infrared Physics and Technology, 111 (2020), 103527.

[24] A. Scalbi, F. Bozzoli, L. Cattani, G. Inglese, M. Malavasi, R. Olmi, *Thermal imaging of inaccessible interfaces,* Infrared Physics and Technology, 125 (2022).

[25] P. Shyprykevich, J. Tomblin, L. Ilcewicz et al., *Guidelines for analysis, testing, and nondestructive inspection of impact damaged composite sandwich structures,* report DOT/FAA/AR-02/121 Office of Aviation Research Washington, D.C.

[26] I. Tougri, M.J. Colaco, F. Bozzoli, L. Cattani, *Internal heat transfer coefficient estimation in three-dimensional ducts through the reciprocity functional approach: analytical approach and validation with experimental data,* International Journal of Heat and Mass Transfer, 122 (2018), 587-601.